Exploring a new role of cyclic and acyclic ionophores in the Potentiometric Recognition of Organic Drug Molecules beyond metal ions: Case Study with Ephedrine hydrochloride

Marwa Alsulaimany [a], Claire Simons [b], Nehad A. Abdallah* [a]

[a] *Pharmacognosy and Pharmaceutical Chemistry Department, College of Pharmacy, Taibah University, Al-Madinah Al-Munawarah, 30078, KSA.*

[b] *School of Pharmacy and Pharmaceutical Sciences, Cardiff University, King Edward VII Avenue, Cardiff, CF10 3NB UK.*

* Corresponding author:
E-mail address: nehad.amin@gmail.com
ORCID ID: (https://orcid.org/0000-0001-5662-2173)
Tel: +966-56-0034928

Abstract

In electrochemical sensing platforms, monensin sodium and nonactin ionophores have been extensively used for the selective recognition of metal cations. The objective of this research is to study and compare their potential for the selective potentiometric detection of ephedrine hydrochloride, a small organic cation. Ephedrine hydrochloride was chosen because of its small molecular size and flexibility, which facilitate its incorporation and binding with ionophores. To measure the concentration of ephedrine hydrochloride, two carbon paste electrodes were designed, where monensin sodium (carbon paste electrode 1) and nonactin (carbon paste electrode 2) served as recognition elements. A combination of CuO and multiwalled carbon nanotubes was employed as an ion-to-electron transducer. The electrodes' selectivity, sensitivity, and response toward ephedrine hydrochloride were evaluated according to IUPAC guidelines. The studied electrodes showed linearity over the concentration ranges of 1×10^{-3} M to 1×10^{-5} M and $\times 10^{-2}$ M to 1×10^{-7} M with LOD values of 5×10^{-6} M and 9×10^{-8} M, for electrodes 1 and 2, respectively. They exhibited high stability for approximately 73 and 95 days, respectively, with no surface renewal action. Both electrodes were used to measure the concentrations of ephedrine hydrochloride in spiked human plasma, pure form, and in different pharmaceutical dose forms.

Keywords: Monensin; Nonactin; Ephedrine; Carbon Paste Electrode; MWCNTs; Potentiometry.

1. Introduction

The potentiometric technique is widely used for determining specific ions by measuring the voltage of an electrochemical cell. This technique is commonly applied in several disciplines, such as chemistry, biology, and environmental science [1]. Among the benefits of potentiometric analysis are its broad concentration range, affordability, quick response time, low detection limit, ease of preparation, on-site analysis, great selectivity, good repeatability, and extended lifespan [1, 2]. Ion-selective electrodes (ISEs) are typically made of a solid-state, glass, or membrane component that selectively interacts with a target ion. The most important element of ISEs with respect to selectivity is the ionophore, an organic or inorganic compound that binds to the ions under investigation [3]. Introducing a selectively binding ionophore into the ISE sensing layer reduces the overall free energy for ion transfer into the organic phase, as the ion preferentially binds to the ionophore. Moreover, the stronger the ionophore binds to an ion, the greater its effect on the ion's phase transfer equilibrium [4]. Certain ionophore characteristics have been found to have a significant effect on molecular binding properties. It includes structural flexibility, binding site geometry, molecular topology, and binding interactions such as hydrogen bonding, charge, and π-electron interactions [5, 6].

Monensin sodium is a polyether antibiotic derived from *Streptomyces cinnamonensis*. Its chemical structure is characterized by a flexible, open polyether backbone that includes multiple oxygen atoms capable of coordinating with cations [7, 8]. Monensin's unique structure allows it to form stable complexes with a variety of monovalent cations, including sodium, potassium, and lithium [7, 9-12]. Tetrahydrofuran and tetrahydropyran rings' oxygen atoms constitute the binding sites in the monensin structure, which help move these cations across lipid membranes. It functions primarily as a sodium /Hydrogen antiporter, exchanging sodium ions for protons and thereby affecting cellular ion balance [13].

Nonactin is a macrotetrolide that is naturally occurring and has been identified as a potential carrier of metal cations, ammonium, and protonated amines. The encapsulation of the cation within the cavity of nonactin is facilitated by the oxygen atoms from the oxolane and ester linkages of the macrocycle backbone [14]. Nonactin complexes can incorporate guest cations into organic phases and serve as an essential model for controlling ionic transport through cell membrane lipid bilayers, resulting in selective antibiotic action due to the tight coordination of charged N-H+ bonds of ammonium with the ether oxygen atoms of nonactin's oxolane rings. Furthermore, the coordination arrangements with cations involve a more active action of the oxygen atoms found in the ester carbonyl groups of the macrocycle [15-17].

Monensin sodium and nonactin are known for their selective binding properties and offer different structural advantages that make them suitable for binding small cations, e.g., Na^+, $K^{+,}$ and NH_4^+ ions. Despite their extensive use as metal ionophores, a notable gap exists in the literature regarding their application as ionophores for organic cations. This presents an opportunity for novel research into the broader applications of monensin sodium and nonactin, particularly in the context of organic cation recognition.

The small molecular size and flexible structure of ephedrine hydrochloride (EH) make it an ideal candidate for binding with different recognition ionophores in potentiometric electrodes. Its amino group, along with the molecular geometry, allows it to interact efficiently with ionophores, facilitating electron transfer at the electrode surface. The molecule's rotatable bonds enable it to adopt various conformations, facilitating efficient binding interactions. Additionally, the small size of EH ensures that it can easily fit into the binding cavity of ionophores, enhancing the stability and specificity of the complex [18, 19]. This makes ephedrine a useful model for researching the interaction between organic cations and the examined ionophores, providing significant insights into the prospective applications of monensin sodium and nonactin ionophores outside their typical employment with metal cations.

Ephedrine hydrochloride (EH) ((1*R*,2*S*)-2-(methylamino)-1-phenylpropan-1-ol; hydrochloride) is an alkaloid mainly found in the species *Ephedra sinica*. Ephedrine, a sympathomimetic amine, is most typically used as a decongestant and nutritional supplement for weight reduction and energy boosting [20, 21]. EH stimulates thermogenesis in humans and is used to improve the performance of athletes. The toxicity of this amine can cause paranoid psychosis, delusions, and hallucinations [21].

Given its role in the nervous system, its wide medicinal use, and potential for misuse, detecting and monitoring ephedrine levels in pharmaceutical and biological samples is critical. Different analytical techniques were published in the literature for the determination of EH. These methods are spectrophotometry [22-25], spectrofluorimetry [26], HPLC [24, 27-30], LC/MS [31, 32], GC/MS [33-35], capillary electrophoresis [36-38], and electrochemistry [39-45]. Most of the reported methods need well-equipped laboratories and experienced staff, while also being costly and time-consuming.

.

In this study, potentiometric sensors were designed for the determination of EH. Solid-contact ion-selective electrodes (SC-ISEs) are substantially more stable than traditional liquid-contact ion-selective electrodes. SC-ISEs eliminate the demand for internal liquid junctions, reducing the potential of liquid leakage and signal drift over time. This leads to more reliable and consistent measurements [46, 47]. Carbon paste electrodes (CPEs) are favored in electrochemical sensing due to their ease of preparation, low cost, and broad potential window. CPEs are generally made up of a recognition element, which determines their selectivity, and a transducer, which converts the recognition ion into a signal with an appropriate sensitivity. By modifying CPEs with ionophores, selective recognition of specific analytes can be achieved. This approach improves the electrode's sensitivity and selectivity toward the target molecule [48-50].

The suggested CPEs have been made using a combination of copper oxide nanoparticles (CuO-NPs) and multi-walled carbon nanotubes (MWCNTs) as an ion-to-electron transducer. Because of their superior mechanical and electrical qualities, carbon nanostructures are efficient transducers in a variety of electrochemical processes [51, 52]. MWCNTs are enriched with metal oxide nanoparticles to increase their surface area, which creates more active sites for ion adsorption and electron transfer, in addition to improving their electrical and thermal conductivity and electron transfer rate [53-57].

This study aims to compare the binding efficiency of an open-structure ionophore, monensin sodium, and a closed-structure ionophore, nonactin, to organic cations. Two carbon paste electrodes were designed, each incorporating either monensin sodium or nonactin, and their performance was evaluated in the quantitation of EH in different matrices. By comparing the binding efficiency and selectivity of open and closed structure ionophores, this work could broaden the range of applications of such ionophores in pharmaceutical analysis. The potentiometric response of these CPEs was monitored following IUPAC recommendations [58]. The studied CPEs were used to measure EH in pure form, in pharmaceutical formulations, and in spiked human plasma.

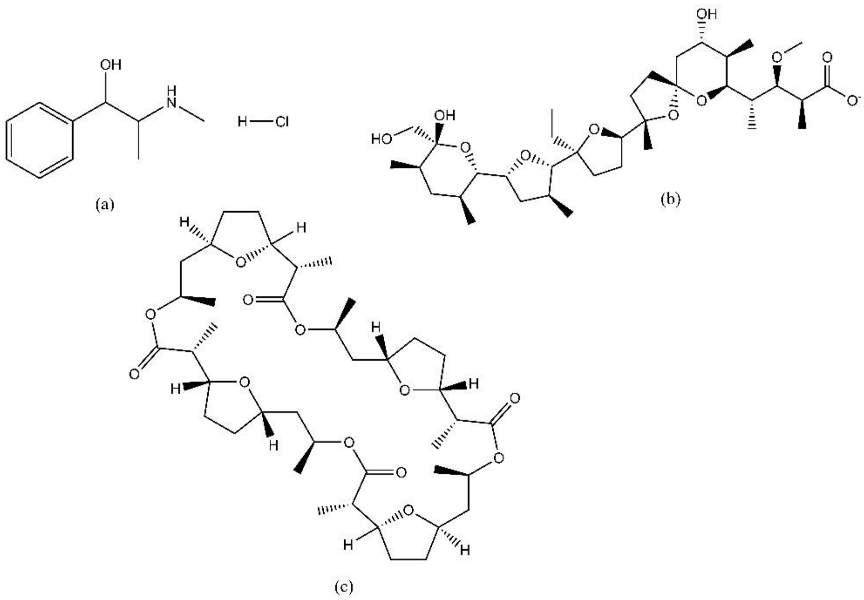

Fig.1. Chemical structures of (a) ephedrine hydrochloride, (b) monensin sodium, (c) nonactin

2. Procedure

2.1. Reagents and chemicals

Ephedrine hydrochloride standard material (B.no. S44211V) was purchased from Sigma-Aldrich, India. Graphite (B.N. MKCC3878), "multi-walled carbon nanotubes (MWCNTs)" (MKBT4011V, 70-80% Carbon content, O.D.× I.D. × L = 10 nm × 4.5 nm × 4 μm), "copper oxide nanoparticles" (544868-5G, nanopowder, % copper 77.0 - 82.6 %, <50 nm particle size), and monensin sodium (B.N. 117K5006V) were supplied from Sigma-Aldrich, USA. Nonactin was obtained from Merck. Paraffin oil was obtained from Fluka. LOBA Chemie PVT. LTD. provided potassium tetrakis (4-chlorophenyl) borate (KTCPB) (B.N. B300171904).

2.2. Instrumentation

CLEAN digital ion analyzer PH 600, model 007747 (China) and Heidolph MR Hei-Standard, magnetic stirrer model 100818877 were used for potentiometric measurements. To create an electrochemical cell, the fabricated CPE was connected to a Thermo-Orion double junction Ag/AgCl reference electrode No. 900201. The CPE body was purchased in China from the Minihua store.

2.3. Preparation of the proposed CPEs

The transducer, MWCNTs/CuO nanocomposite, was prepared as mentioned in our previous work [54, 59]. In brief, pristine MWCNTs were acidified with a mixture of concentrated HNO_3 and H_2SO_4 (1:3 v/v) with ultrasonication for 3 hrs, followed by reflux at 70 °C. The carboxylated MWCNTs were filtered and vacuum dried at 70°C. In 50 mL of *N, N-dimethylformamide*, 50 mg of the carboxylated MWCNTs were mixed with CuO nanoparticles. In order to dissolve both components and effectively coat the CNTs' surface with metal oxide nanoparticles, the mixture was ultrasonically agitated for 72 hours at room temperature. For a duration of 48 hours, the solution was vacuum-dried at ambient temperature.

Graphite powder, MWCNTs/CuO, ionophore, KTCB as a lipophilic cation exchanger, and paraffin oil were mixed uniformly in a 52: 8: 6: 4: 30% w/w ratio to fabricate the CPEs. Monensin sodium and nonactin were used as the recognition ionophores in CPE1 and CPE2, respectively. The resulting mixture was packed carefully into the electrode body, ensuring a smooth surface with a tracing paper for uniform electrochemical measurements.

2.4. Study the selectivity of the proposed CPEs

The matched potential method was applied to assess the CPEs' selectivity in the presence of interferents and compounds with comparable structures. The exact concentrations of the primary ion (EH) and the interfering ion that produce an equivalent change in the potential value of the reference solution under the identical circumstances were used to calculate the selectivity coefficient ($K^{pot}_{EH,\ interferent}$). Equation (1) is used to calculate the selectivity coefficient in compliance with IUPAC guidelines [58].

$$K^{pot}_{(A,\ B)} = \frac{a'_A - a_A}{a_B} \quad (1)$$

EH and interfering ions are represented by the letters A and B, respectively. The activity of the reference solution of EH is represented by the symbol a_A. A solution of 1×10^{-4} M of EH was utilized as the reference solution. a'_Arepresents the activity of the added EH to the reference solution and produces a potential change (ΔE). While a_B is the interfering ion's activity, which, when added to the same reference solution of EH, produces the same potential change (ΔE) as produced by adding a known increment of the primary ion.

2.5. Conductometric analysis of the interaction of ionophores and EH.

The interaction between EH, the target molecule, and monensin and nonactin as ionophores was investigated using a conductometric titration. Conductance measurements were carried out under thermostatically controlled temperature at 25 ℃ using a Clean CON500 meter with a conductivity sensor and a cell constant of 0.99 ± 0.01 cm^{-1}. 25 mL of 1 × 10^{-2} M of EH was prepared in 0.01 M Britton-Robinson buffer at pH 6 for monensin sodium titration and at pH 7 for nonaction titration. A known amount of the concentrated ionophore was added stepwise by means of a micropipette. The conductivity was measured following each addition after the solution had been magnetically stirred for approximately one minute.

2.6. Computational study

The ionophore-ephedrine complexes were prepared using the Builder tool in the Molecular Operating Environment (MOE) software [60]. The charges of EH (+1), nonactin (0), and monensin A (-1) were set, then the two ionophore-ephedrine systems were prepared through partial charges and energy minimisation (Gradient 0.1 RMS kcal/mol/Å2) using the MMFF94x forcefield.

Molecular dynamics (MD) for the solvent-free systems was performed on both ionophore-EH complexes at 300K using the NPA algorithm and a protocol of initial equilibration for 100 ps followed by a production step for 1100 ps for a total MD simulation time of 1200 ps. For MD simulations of the solvated ionophore-EH complexes, the mode of solvation (H_2O, Periodic, Cube) was set, followed by computing partial charges and energy minimisation (Gradient 0.1 RMS kcal/mol/Å2) of the solvated systems. The MD protocol was as described for the solvent-free system, with an initial equilibration for 100 ps followed by a shorter production step for 400 ps for a total MD simulation time of 500 ps. Full details of the MD protocols are provided in Supporting Information **(S1).**

2.7. Application of the proposed CPEs

The EH concentration in syrups and tablets was measured using the proposed sensors. After being weighed, each of the twenty tablets was ground into a fine powder. To prepare a standard solution of 1 x 10^{-2} M of EH, a precisely weighed quantity of the ground tablets was put into a 50 mL volumetric flask, diluted in a small amount of acetonitrile, and then filled to the mark with 0.01 M Britton-Robinson buffer. The standard solution was diluted with Britton-Robinson buffer to produce a range of EH concentrations, from 1 × 10^{-3} M to 1 × 10^{-8} M.

In order to prepare 1 × 10^{-2} M of EH, 10 bottles of Sudophine syrup were mixed uniformly, and a specific volume of the syrup was then transferred to a 50 mL volumetric flask and diluted to the appropriate level with 0.01 M Britton-Robinson buffer. As previously stated with the tablets, various dilutions were prepared.

For plasma samples, 1 mL of acetonitrile was added for protein precipitation after 0.5 mL of plain plasma had been spiked with 0.5 mL of various concentrations of standard EH solutions. For five minutes, the samples were centrifuged at 7000 rpm. 1 mL of the supernatant was placed into a 10 mL volumetric flask and diluted with 0.01 M Britton-Robinson buffer solution. After plotting the calibration curve, the impact of the plasma matrix on the electrode response was calculated using the following equation [61]:

$$ME\ \% = 100\ \times (\frac{S_m}{S_a} - 1) \quad (2)$$

where S_a and S_m stand for the calibration curve's slope in the plasma and the aqueous medium, respectively. The corresponding correlating regression equation for each type of sample was used to measure the concentration of EH samples.

3. Results and discussion

3.1. Evaluation of the recognition of the ionophores to the target EH molecule

3.1.1. conductometric titration

The interaction between the studied ionophores and EH is confirmed by plotting the molar conductance-mole ratio curve. **Fig.2** represents the relation between the conductance (Λm) and mole ratio of EH and monensin sodium, and nonactin, separately. It was found that the conductance decreased gradually with the addition of each ionophore. A breakpoint in the conductivity plot indicates complex formation, and it was levelled out at a molar ratio of 1:1 for [ionophore: EH] in the formed complex. The formed complex exhibits less mobility in solution than the uncomplexed EH, resulting in a decreased capacity for charge transport and, consequently, a low conductivity of the solution. In the case of nonactin, the molar conductance did not significantly change with the addition of the ionophore after the complex formation. While for monensin A, a slight increase in the conductance is observed after the complex formation due to the presence of ionized monensin.

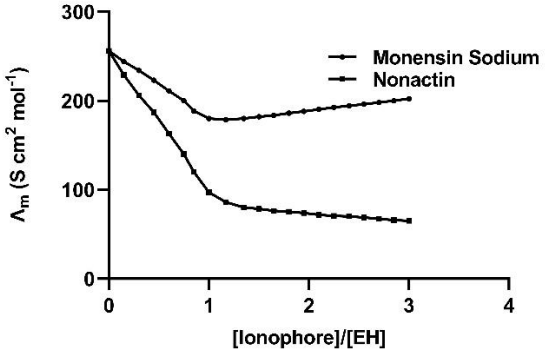

Figure 2. Conductometric titration of 1×10^{-3} M of EH with monensin sodium and nonactin at 25 °C.

3.1.2. Molecular dynamics (MD) simulations

To demonstrate the novelty of this work, a MD simulation showed a promising binding interaction between the two ionophores and EH. The monensin-ephedrine complex final frame showed ionic interactions between the carboxylate anion of monensin and the protonated amine of ephedrine, as well as H-bonding between the lone pair of the OH group of monensin and the charged amine (**Fig. 3a**). Furthermore, the overlapping trajectories illustrate the stability of the monensin-EH complex during a 1200 ps simulation time and the flexibility of the acyclic ionophore to form a cavity/pocket for binding with ephedrine (**Fig. 3b**).

For the cyclic ionophore (nonactin), the MD simulation represented H-bonding between the protonated amine of EH and the carbonyl O of nonactin in addition to H-bonding between the OH group of ephedrine and the furan O of nonactin, as shown in **Fig. 3c**. The nonactin-ephedrine overlapping trajectories confirmed very consistent positioning of EH during the simulation time (Figure 3d). The

simulation results confirmed the sensitivity of EH to both ionophores, with minimal preference for nonactin.

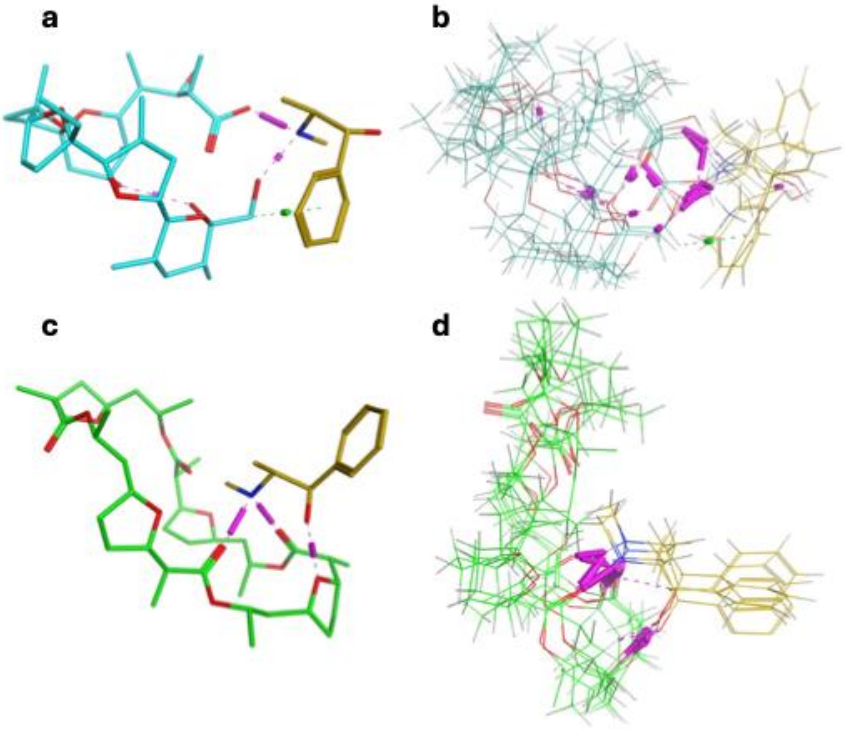

Figure 3: A 3D representation of EH (gold) forming H-bonding and ionic interactions with (a) monensin (cyan) and (c) nonactin (green) in the final frame of the 1200 ps MD simulation. Overlapping several trajectories from the MD simulation at 600, 850, 1100, and 1200 ps showed reasonable overlap for (b) monensin-EH complex and close overlap and conformational stability for (d) nonactin-EH complex.

To more closely represent the experimental aqueous conditions, a further 500 ps MD simulation of the ionophore-EH complexes was run, including water of solvation.

In the case of the monensin-EH complex, EH moved away from the initial placement with a loss of any direct binding interactions between the ionophore and EH at the end of the simulation time (**Fig. 4a**). Overlap of trajectories at 100, 350, and 500 ps showed a mobile system potentially owing to the greater flexibility of the acyclic monensin and solvation of the carboxylate anion, reducing interaction with EH.

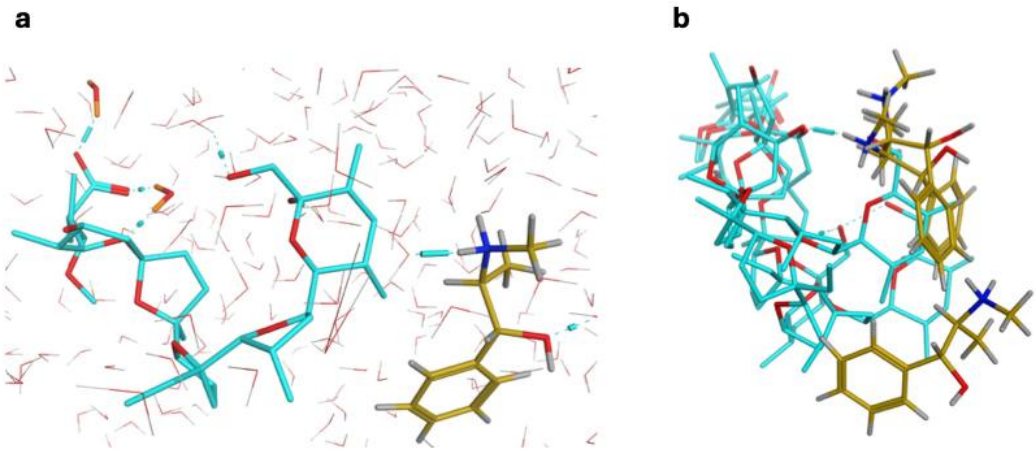

Figure 4. Monensin-EH complex (a) final frame after 500 ps MD simulation illustrating dispersion of EH (gold) away from monensin (cyan) and solvation of the carboxylate anion of monensin (two H_2O molecules shown in orange) (b) Overlap of MD simulation trajectories at 100, 350 and 500 ps showing movement of both monensin (cyan) and EH (gold) [H_2O molecules hidden for clarity].

For the nonactin-EH complex, ephedrine formed two H-bonds between the protonated amine and two carbonyl groups of nonactin, while the hydroxy group of EH formed H-bonds between one carbonyl group and water of solvation (**Fig. 5a**). Overlap between trajectories at 100, 350, and 500 ps showed consistent placement and stability throughout the MD simulation (Figure 5b). Nonactin was shown to encapsulate EH within its structure, as illustrated with the space-filled model in Figure 5c. The molecular dynamics protocol was represented as Supplementary **S1**.

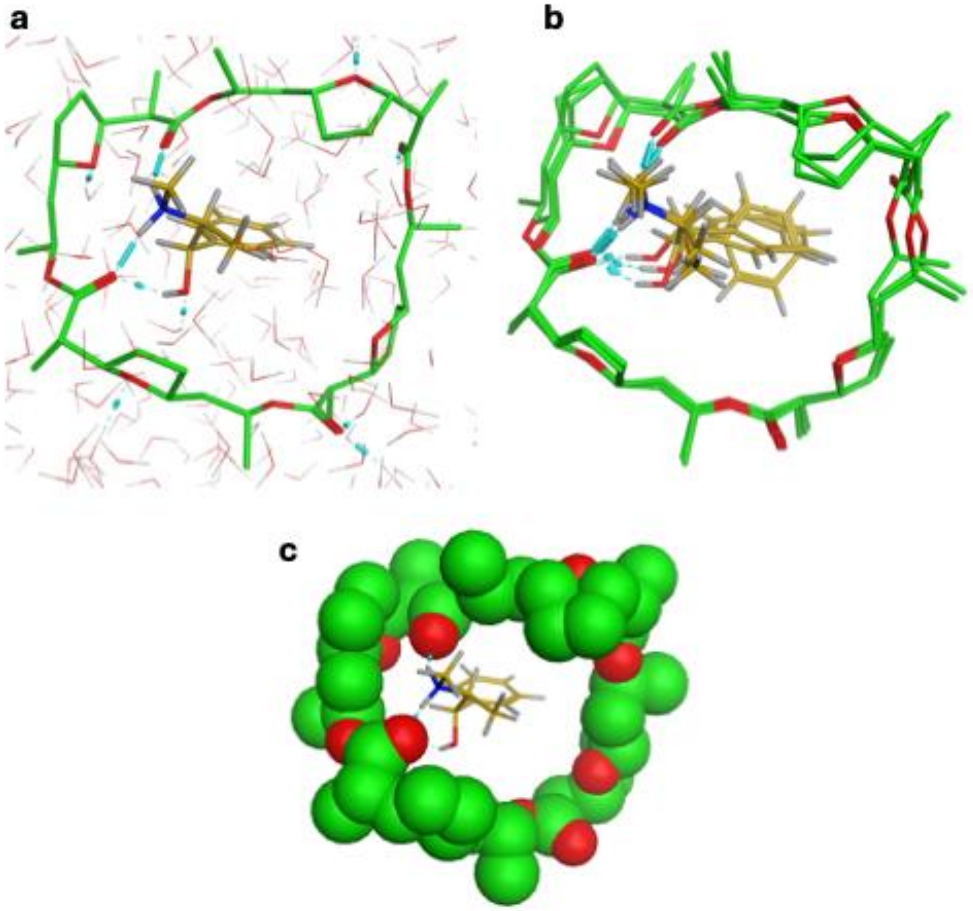

Figure 5. Nonactin-EH complex (a) final frame after 500 ps MD simulation illustrating H-bonding interactions between EH (gold) and nonactin (green) (b) Overlap of MD simulation trajectories at 100, 350, and 500 ps showing consistency of the complex [H_2O molecules hidden for clarity] (c) Space-filled image of nonactin (green) encapsulating ephedrine (gold).

3.2. Characterization of the prepared transducer nanocomposite

CuO was chosen as the metal oxide component of the transducer layer because it provides excellent electrical conductivity, chemical stability, and strong redox activity that promote efficient ion-to-electron charge transfer at the electrode interface [62]. In the fabricated MWCNTs/CuO composite, CuO nanoparticles are uniformly distributed over the surface of multi-walled carbon nanotubes (MWCNTs), as confirmed by FT-IR and XRD analysis. This hybrid structure combines the large surface

area and high electron mobility of the nanotubes with the semiconducting and catalytic nature of CuO, resulting in a synergistic transduction mechanism [62, 63].

Specifically, CuO nanoparticles act as redox mediators that facilitate the electron transfer between the ion-recognition sites and the carbon matrix. The Cu^{2+}/Cu^{+} redox couple readily exchanges electrons, enabling rapid charge transfer through the carbon paste to the underlying conductive metal. Meanwhile, the CuO coating stabilizes the dispersion of the nanotubes and prevents their aggregation, maintaining an extensive electroactive surface. This dual function enhances the sensitivity, response time, and lifetime of the sensor compared to unmodified CNT electrodes [62, 63]. Moreover, CuO enhances the hydrophilicity of the transducer surface, ensuring intimate contact between the ionophore phase and the electronic substrate, which minimizes potential drift and improves long-term stability.

The oxidized MWCNTs' FT-IR spectrum, shown in **Fig. 6(a)**, showed an absorption band at 1725 cm^{-1} that corresponds to C=O stretching of the COOH group and a large band at 3467 cm^{-1} that corresponds to O-H stretching. The intrinsic structure of CNTs exhibits a C=C stretching band at 1550 cm^{-1}. Bands at 1388 cm^{-1} and 1078 cm^{-1}, respectively, represent O-H bending and C-O stretching vibrations. It guaranteed the MWCNTs' effective oxidation.

Two absorption bands at 538 cm^{-1} and 1010 cm^{-1} in the FT-IR spectrum of CuO nanoparticles in **Fig. 6(b)** are associated with the stretching vibrations of the Cu-O bond. This demonstrates the existence of metal oxide linkages that identify the CuO nanoparticle structure as documented in the literature [54, 64].

Fig. 6(c), the carboxyl group's band shifted and shrank in the MWCNTs-CuO nanohybrid spectrum, suggesting that it was utilized for attaching to CuO nanoparticles. The nanohybrid displayed a band at 1631 cm^{-1} of the Cu-O stretching vibration and two absorption bands at 538 cm^{-1} and 1024 cm^{-1} of the Cu-O bending vibrations.

The oxidized MWCNTs' XRD in **Fig. 7(a)** revealed a strong band at 2θ of 28.5° of the hexagonal graphite structure's diffraction. Intense diffraction peaks at 2θ of 32.9°, 35.8°, 38.5°, 49.6°, 54.9°, 59.8°, 63.1°, 68.1°, and 69.6° corresponding to the crystal planes of CuO nanoparticles were observed in **Fig. 7(b)**. Both CuO nanoparticles and oxidized MWCNTs had diffraction peaks that were consistent with those found in the literature [62]. The strong MWCNTs diffraction peak at 25.7° overlapped with the CuO nanoparticle diffraction peak in the MWCNTs-CuO nanohybrid diffraction pattern, **Fig. 7(c)**. The last distinctive CuO peaks were seen. This demonstrates that MWCNTs were successfully functionalized using CuO nanoparticles.

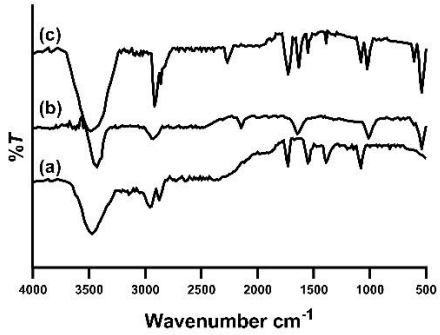

Fig. 6. FT-IR spectra of (a) the oxidized MWCNTs, (b) CuO nanoparticles, and (c) MWCNTs/CuO nanohybrid

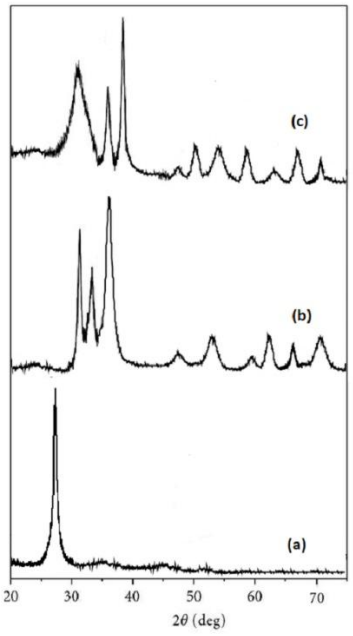

Fig. 7. XRD of (a) the oxidized MWCNTs, (b) CuO nanoparticles, and (c) MWCNTs/CuO nanohybrid

3.3. Optimum composition of the designed CPEs

Table 1 illustrates the manufacture of CPEs utilizing various paste compositions in sequential steps to attain the optimal formulation of the proposed sensors. The nonactin ionophore served as a model recognition element to determine the optimal electrode composition. A consistent mixture of 70% w/w graphite powder and 30% w/w paraffin oil, used as a binder, produced a homogeneous and long-lasting paste. As a lipophilic ionic exchanger, KTCPB enhances the potentiometric slope and other response properties. The lipophilic additive of opposite charge to EH ensures that enough analyte ions can be extracted into the paste, with all counterions being excluded [3]. The electrode containing KTPCPB (sensor 2) without the ionophore showed a noticeably lower slope (48.56 mV/decade) and narrower linear range compared with the ionophore-containing electrode (sensor 3), confirming the essential role of the ionophore in improving the electrode response. Moreover, ionic sites in the carbon paste lower its electrical resistance, facilitating the ionic mobility inside the paste. Sensors 4, 5, and 6 were created by combining varying amounts of nonactin and KTCPB. The influence of the MWCNTs/CuO percentage as a transducer was investigated using three sensors (sensors 7, 8, and 9). Combining graphite, paraffin oil, MWCNTs/CuO, ionophore, and KTCPB in a ratio of 52:30:8:6:4% (w/w) provided the best performance. When designing the other CPE using the monensin sodium ionophore, this ratio was taken into account. The present work aimed to investigate the effect of the type of ionophore on the electrode performance while keeping the other composite components constant. Accordingly, the optimization process was first conducted using nonactin to reach the best formulation (sensor 8). This optimized composition was then used as a reference formulation in which only the ionophore was replaced by monensin (sensor10). This design allowed direct comparison of the two ionophores under identical experimental conditions and clearly demonstrated the influence of the ionophore nature on the analytical performance of the carbon paste electrode.

Table 1. The effect of the electrode composition on its potentiometric performance

	Graphite (% w/w)	MWCNTs/CuO composite (% w/w)	Nonactin (%w/w)	KTCPB (% w/w)	Paraffin Oil (%w/w)	Linearity range (M)	LOD (M)	Slope (mV/decade)	Response time (s)
1	70	-	-	-	30	7×10^{-1} - 1×10^{-1}	1×10^{-2}	23.87	120
2	60	-	-	10	30	1×10^{-2} - 1×10^{-1}	1×10^{-2}	48.56	100
3	60	-	10	-	30	5×10^{-3} - 1×10^{-1}	$3 \times 1\ 0^{-4}$	49.78	90
4	60	-	8	2	30	1×10^{-3} - 1×10^{-1}	$4 \times 1\ 0^{-4}$	52.67	75
5	60	-	6	4	30	1×10^{-4} - 1×10^{-1}	2×10^{-5}	51.16	60
6	50	-	4	6	30	1×10^{-3} - 1×10^{-1}	5×10^{-4}	53.33	45
7	50	10	6	4	30	1×10^{-6} - 1×10^{-3}	3×10^{-7}	55.26	12
8	**52**	**8**	**6**	**4**	**30**	**1×10^{-7}- 1×10^{-2}**	**9×10^{-8}**	**59.07**	**7**
9	54	6	6	4	30	1×10^{-6} - 1×10^{-2}	8×10^{-7}	56.04	10
10	**52**	**8**	**6 (Monensin)**	**4**	**30**	**1×10^{-5}- 1×10^{-3}**	**5×10^{-6}**	**57.82**	**15**

3.4. Potentiometric response characteristics of the designed CPEs

In this work, two CPEs with different ionophores, monensin sodium (CPE 1), and nonactin (CPE 2), were developed and used for the selective determination of EH. The potentiometric response of these sensors was studied according to IUPAC measures [54] and summarized in **Table 2**.

With Nernstian slopes of 57.82 ± 0.61 and 59.07 ± 0.34 mV/decade, respectively, the sensors demonstrated linear response over 1×10^{-5} to 1×10^{-3} M and 1×10^{-7} to 1×10^{-2} M of EH for CPE1 and CPE2, as illustrated in **Fig. 8**. The sensitivity of CPE2 was higher, with a LOD of 9×10^{-8} M. Without surface renewal of the electrode paste, the calibration slope, linearity range, and reaction time of the proposed CPEs were continuously tracked to determine their stability. For CPE 1 and CPE 2, the electrode response was within ± 1.5% of their initial values after 73 and 95 days, respectively. The long-term stability of the proposed CPEs (CPE-1 and CPE-2) is expressed as slope (mV/decade) versus time in and represented in **S2**.

Three quality-control standards (1×10^{-3} M, 1×10^{-4} M, and 1×10^{-5} M) were used to test the electrodes' precision. Both the intra-day and inter-day RSD were less than 1.8%. For every CPE under investigation, three independently made sensors were used to assess reproducibility under identical conditions; the RSD was less than 2%. The time needed for the electrode to yield ± 1.5 mV of the initial equilibrium potential value following a 10-fold rise in the analyte concentration is known as the dynamic response time. CPE 2 was found to have the fastest response time within 7 seconds. After a 10-fold drop in EH concentration, the time needed to return to equilibrium values was examined and found to be longer. As illustrated in **Fig. 9**, it took roughly 45 s for CPE 1 and 15 s for CPE 2. It guarantees the designed CPEs' reversibility and quick reaction.

The favourable potentiometric response exhibited by the nonactin- and monensin-based CPEs towards EH can be attributed to their exceptional ionophoric properties and compatibility with the structural and physicochemical characteristics of the ephedrine molecule. Nonactin, a cyclic macrotetrolide, is known for its high affinity toward primary ammonium ions due to its flexible polyether cavity, which can conform to accommodate spherical or near-spherical cations [17]. EH, being a protonated secondary amine in aqueous solution, presents a cationic nitrogen at pH below its pKa value that mimics the steric and charge distribution of ammonium ions. The ability of nonactin to form stable hydrogen bonds and ion-dipole interactions with such positively charged centres, combined with its lipophilicity and membrane compatibility, enables a rapid and Nernstian response of CPE 2. Additionally, nonactin's relatively neutral charge and moderate rigidity allow fast ion-exchange kinetics at the carbon paste interface, contributing to both sensitivity and fast electrode response. Monensin, although primarily recognized as a sodium-selective ionophore, also exhibits measurable interaction with EH. Its carboxylic acid group with a pKa of 4.5 is deprotonated at neutral or mildly acidic pH [13], allowing electrostatic attraction between the anionic carboxylate and the cationic amine of EH. While the

structure of monensin is relatively more rigid due to its polyether backbone and chair-like conformation, it still provides sufficient conformational freedom to enable complexation through both electrostatic and dipole interactions. This underlies its acceptable potentiometric performance, although the steric match with EH is less ideal compared to nonactin, leading to a slightly lower sensitivity. In conclusion, the superior performance of the nonactin-based electrode arises from its structural adaptability and strong host–guest interaction with the cationic form of EH, while the monensin-based electrode benefits from favourable electrostatic interactions but is limited by its more constrained geometry and lower binding constant.

Table 2. The electrochemical response characteristics of the studied CPEs.

Parameter	Monensin-based CPE (CPE 1)	Nonactin-based CPE (CPE 2)
Concentration range (M)	$1\times10^{-3} - 1\times10^{-5}$	$1\times10^{-2} - 1\times10^{-7}$
Slope (mV/decade)	57.82 ± 0.74	59.07 ±0.34
Intercept	219.51 ± 1.56	274.18 ± 1.42
Correlation coefficient (r)	0.995	0.998
LOD (M)	5×10^{-6}	9×10^{-8}
Response time (s)	15 ± 2.5	7 ± 1.3
Stability (days)	73	95
Working pH range	5.5 - 7	6 – 8
Average recovery[1]	97.08 ± 1.21	99.42 ± 0.37
Intraday precision[2] (RSD %)	1.35	0.77
Interday precision[2] (RSD %)	1.46	0.86
Reproducibility[3] (RSD %)	1.96	1.52

[1] The mean of five measurements taken at five different concentration levels.
[2] The mean of five determinations of three QC samples.
[3] The mean of five determinations of three QC samples using three independently fabricated sensors.

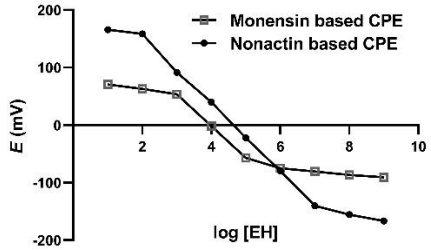

Fig. 8. The potentiometric response of the studied CPEs

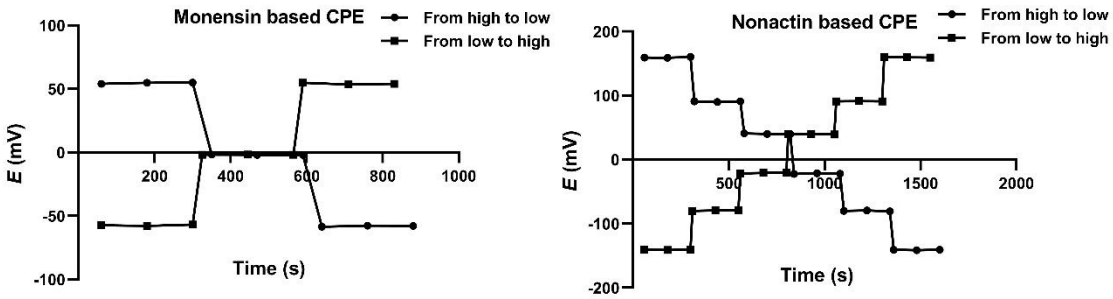

Fig. 9. The dynamic response time of the studied CPEs from low to high and high to low concentrations of EH using the concentration range of 1×10^{-3} to 1×10^{-5} M for monensin-based CPE and 1×10^{-2} to 1×10^{-7} M for nonactin-based CPE.

3.5. pH effect on the response of the CPEs

The response of the designed sensors and the efficient recognition of EH by the ionophores are influenced by the pH of the medium. In order to examine the influence of pH, standard solutions of 1×10^{-4} and 1×10^{-5} M EH were prepared at various pH values, extending from 2 to 10. **Fig. 10** illustrates that CPE 1 and CPE 2 maintained consistent measurements within the ranges of 5.5 to 7 and 6 to 8, respectively. Consequently, pH 6 and pH 7 were selected as the recommended pH values for monensin-based CPE 1 and nonactin-based CPE 2, respectively.

As mentioned previously, the complexation mechanism of binding each of nonactin and monensin with EH depends on their molecular architecture, cavity size, and binding preferences, all of which are pH dependent. EH, a basic compound with a pKa around 9.6, exists predominantly in its protonated (cationic) form at physiological and mildly acidic pH values, making it highly suitable for interaction with electron-rich or anionic binding sites [19]. Monensin sodium, a polyether ionophore with a carboxylic acid group with a pKa of 4.5, binds cations through coordination to its ether oxygens and electrostatic interaction with its deprotonated carboxylate. Monensin is structurally flexible, which is essential for forming conformationally adaptive binding pockets around small metal cations [8]. Importantly, below pH 4.5, the carboxyl group is protonated, impairing electrostatic binding. At a pH above 4.5, deprotonation occurs, and monensin can engage in electrostatic attraction with the protonated amine group of EH. Nonactin, a macrotetrolide antibiotic, features a macrocyclic structure with oxygen-rich internal cavities that show high affinity for protonated amines and monovalent cations through hydrogen bonding and dipole–cation interactions. Its flexible ring structure accommodates the sterically hindered protonated nitrogen of EH effectively. Since nonactin is a neutral molecule and lacks ionizable groups in the working pH range (4–7), its binding is largely pH-independent, provided that EH remains in its cationic form, which it does well below its pKa. This makes nonactin an excellent candidate for stable and selective complexation.

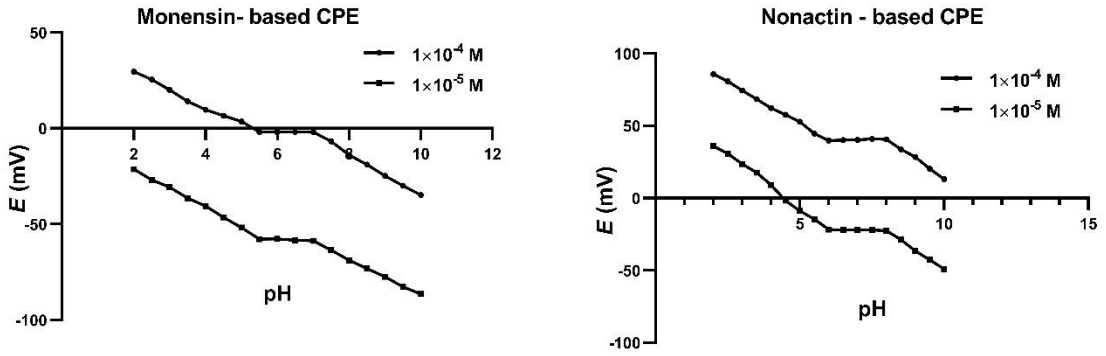

Fig. 10. The influence of pH on the potentiometric response of the studied CPEs using 1×10^{-4} M and 1×10^{-5} M of EH

3.6. Selectivity Study

The matched potential approach was used to evaluate the selectivity of the tested CPEs. The procedure entailed calculating the change in potential (ΔE) after mixing a reference solution of 1×10^{-4} M EH with a known volume of EH solution (aA') and the interfering ion solution (aB), which generates an equal change in the CPE potential (ΔE). The IUPAC recommendation was followed in the determination of

the selectivity coefficient [54]. In the presence of additional interferents, the selectivity coefficient values in **Table 3** show the efficiency of CPE 1 and CPE 2 in selecting EH.

.

Table 3. Potentiometric selectivity coefficient ($\log K^{pot}_{EH,\ Interferent}$) for the studied CPEs

Interfering ions	$\log K^{pot}_{EH,\ Interferent}$	
	Monensin- based CPE (CPE 1)	**Nonactin-based CPE (CPE 2)**
NaCl	-2.33	-3.01
KCl	-2.98	-2.65
NH_4Cl	-3.01	-2.94
Chlorpheniramine	-3.55	-3.12
Caffein	-3.98	-4.33
Aspirin	-3.75	-4.04
Paracetamol	-3.93	-3.91
Dopamine HCl	-4.13	-3.98

A review of the response characteristics of the suggested CPEs compared to the reported ones [39, 41, 45] is represented in **Table 4**. One of the sensors reported in the literature was a traditional liquid contact ISE, with a PVC membrane positioned between the sample and an internal filling solution [41] or the PVC polymeric membrane is drop-cast over the electrode surface [39, 45]. The main challenges facing these traditional liquid contact ISEs are their fragility, difficulty in downsizing, the need for extra maintenance since the inner filling solution evaporates, and the gradual leaching of some membrane components. Each of these elements has a passive impact on the ISE's sensitivity and stability. The results confirmed that the nonactin-based CPE (CPE 2) exhibited a remarkable response to EH with a wider linearity range and sensitivity in comparison to the other reported ones. Without any surface renewal procedures, the suggested sensors demonstrated excellent stability and longer lifespans of 73 and 90 days for CPE 1 and CPE 2, respectively. For the same paste, surface renewal might increase the suggested sensors' lifespan three or four times.

Table 4. Comparison of the potentiometric response characteristics between the reported electrodes and the studied ones.

Electrode composition	Linearity range (M)	LOD (M)	Slope mV/decade	Stability	Response time (s)	Ref
Classical liquid contact ISE with a PVC membrane (triacetyl-b-cyclodextrin, plasticizer, PVC and (K-TPB) and dissolved in THF)	$3.1 \times 10^{-5} – 7.9 \times 10^{-3}$	5.7×10^{-6}	57.3	5 weeks	10-20	[41]
Classical liquid contact ISE with a PVC membrane (PVC-COOH, plasticizer, (K-TPB) and dissolved in THF)	$7.2 \times 10^{-5} – 7.9 \times 10^{-3}$	1.7×10^{-5}	57.6	8 weeks	10-20	[41]
Polyaniline modified Glassy carbon electrode drop casted with PVC membrane (tungstophosphoric acid hydrate, tricresyl phosphate, and calix [8] arene)	6×10^{-6} - 1×10^{-2}	3.6×10^{-6}	58.86	30 days	8	[45]
Graphite/epoxy resin electrode coated with a PVC membrane which is formed	2×10^{-5} - 1×10^{-1}	1×10^{-5}	57.5	6 months	6	[39]

of ion pair precipitate of EH and potassium tetrakis (4-chlorophenyl) borate dissolved in THF						
CPE (graphite, paraffin oil, MWCNTs/CuO, Monensin sodium, and KTCPB)	1×10^{-5} - 1×10^{-3}	5×10^{-6}	57.82 ± 0.74	73 days	15	This work
CPE (graphite, paraffin oil, MWCNTs/CuO, nonactin, and KTCPB)	1×10^{-7} - 1×10^{-2}	9×10^{-8}	59.07 ±0.34	95 days	7	This work

3.7. Water layer test

The potential drift caused by the water layer between the carbon paste and the conducting copper element can be detected by the water-layer test [59]. The EH standard solution's potential reading was monitored for three hours. After that, the electrode was exposed to the same concentration of dopamine hydrochloride for three more hours as an interfering ion. After that, it was re-exposed to the EH standard solution for three more hours. After three hours of exposure to the interfering ion, the response of the sensors under study stayed consistent, as shown in **Fig. 11**, demonstrating the absence of a water layer. This may be explained by the hydrophobic nature of the resulting paste, which inhibits the formation of a water layer at the interface between the paste and the conducting surface of the CPE body.

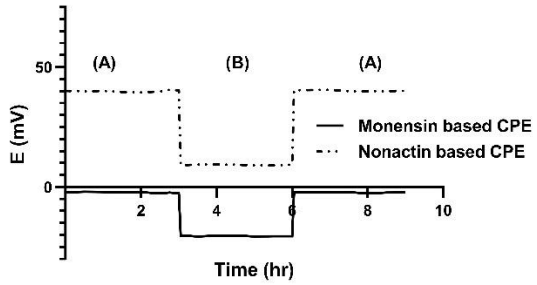

Fig. 11. Water layer test of the studied CPEs. The potential readings at (A) 1×10^{-4} M EH, followed by (B) 1×10^{-4} M dopamine hydrochloride, then (A) 1×10^{-4} M EH.

3.8. Analytical applications

The offered sensors are efficiently applied for measuring EH in different matrices due to their high sensitivity, stability, and broad linearity range. The EH concentration in the pharmaceutical formulation samples was estimated with the standard addition method, whereas in spiked plasma samples, the EH concentration was determined using the corresponding regression equation in plasma. The efficiency and accuracy of the CPEs in the determination of EH in a variety of matrices are demonstrated in **Table 5**.

Table 5. Application of the proposed CPE 1 and CPE 2 for the determination of ephedrine hydrochloride in different matrices.

Sample	Monensin-based CPE (CPE 1)			Nonactin-based CPE (CPE 2)	
	Spiked concentration (µM)	Total found concentration* (µM)	Recovery %	Total found concentration* (µM)	Recovery %
Asmacid tablets	0	9.8	-	10	-

	90	99.5	99.7	100.1	100.1
	990	987.8	98.8	995.7	99.6
	0	9.7	-	9.8	-
Sudophine Syrup	90	93.5	93.1	98.7	98.8
	990	987.8	98.8	994.5	99.5
	10	8.7	87.0	9.5	95.0
Human plasma	100	92.5	92.5	97.7	97.8
	1000	985.4	98.5	996.8	99.7

* Average of three determinations.

The F-test and the Student's t-test at p = 0.05 were used to statistically compare the results obtained by the studied CPEs with those of the reported method [39] for determining EH in both standard solutions and pharmaceutical syrup samples. No significant differences were observed, as shown in **Table 6**, confirming the validity and accuracy of the proposed electrodes

Table 6. Statistical comparison of the proposed CPEs and the reported method

	Sample	Monensin-based CPE. (CPE 1)	Nonactin-based CPE. (CPE 2)	Reported method [39]
Pure Sample	**Recovery %**	98.69	99.73	99.95
	SD	1.03	1.14	0.89
	n	5	5	6
	Variance	1.06	1.29	0.79
	F-test (5.19)*	0.741	0.598	
	Student t-test (2.262)*	2.15	0.35	
Pharmaceutical Syrup	**Recovery %**	99.12	98.42	**98.43**
	SD	1.14	1.23	**1.06**
	n	5	5	**6**
	Variance	1.30	1.51	**1.12**
	F-test (5.19)*	0.853	0.738	
	Student t-test (2.262)*	1.03	0.01	

*The values in parentheses are the theoretical values of t and F at p=0.05.

Conclusion

This study successfully demonstrated a novel application of monensin sodium (acyclic ionophore) and nonactin (cyclic ionophore) as recognition elements in potentiometric sensors for the determination of the small organic cation, EH, expanding their traditional use beyond metallic and ammonium ions. The nonactin-based sensor exhibited superior selectivity, sensitivity, and faster response characteristics compared to the monensin-based sensor, making it the more efficient choice for EH detection. Both sensors were validated and effectively applied to the quantification of EH in pure form, pharmaceutical formulations, and spiked plasma samples, confirming their robustness and analytical applicability. The promising performance of nonactin- and monensin-based sensors for small organic cations opens avenues for developing ionophore-based potentiometric devices targeting other pharmacologically active compounds. Further research could explore structural modifications of ionophores to tailor their binding affinity and selectivity for diverse drug molecules, enhancing their role in pharmaceutical quality control and clinical analysis.

Conflicts of Interest:

There are no conflicts of interest to declare.

References:

[1] J. Bobacka, A. Ivaska, A. Lewenstam, Potentiometric Ion Sensors, Chemical Reviews, 108 (2008) 329-351. 10.1021/cr068100w

[2] M.A. Fathy, P. Bühlmann, Next-Generation Potentiometric Sensors: A Review of Flexible and Wearable Technologies, Biosensors, 15 (2025) 51. https://doi.org/10.3390/bios15010051

[3] R.D. Johnson, L.G. Bachas, Ionophore-based ion-selective potentiometric and optical sensors, Analytical and Bioanalytical Chemistry, 376 (2003) 328-341. 10.1007/s00216-003-1931-0

[4] P. Bühlmann, E. Pretsch, E. Bakker, Carrier-Based Ion-Selective Electrodes and Bulk Optodes. 2. Ionophores for Potentiometric and Optical Sensors, Chemical Reviews, 98 (1998) 1593-1688. 10.1021/cr970113+

[5] M.R. Ganjali, P. Norouzi, M. Rezapour, F. Faridbod, M.R. Pourjavid, Supramolecular Based Membrane Sensors, Sensors, 6 (2006) 1018-1086. https://doi.org/10.3390/s6081018

[6] J. Zhai, D. Yuan, X. Xie, Ionophore-based ion-selective electrodes: signal transduction and amplification from potentiometry, Sensors & Diagnostics, 1 (2022) 213-221. 10.1039/D1SD00055A

[7] A. Huczyński, J. Janczak, D. Łowicki, B. Brzezinski, Monensin A acid complexes as a model of electrogenic transport of sodium cation, Biochimica et Biophysica Acta (BBA) - Biomembranes, 1818 (2012) 2108-2119. https://doi.org/10.1016/j.bbamem.2012.04.017

[8] D. Aowicki, A. Huczyński, Structure and antimicrobial properties of monensin A and its derivatives: summary of the achievements, Biomed Res Int, 2013 (2013) 742149. 10.1155/2013/742149

[9] W. Pangborn, W. Duax, D. Langs, The hydrated potassium complex of the ionophore monensin A, Journal of the American Chemical Society, 109 (1987) 2163-2165. 10.1021/ja00241a038

[10] K. Tohda, K. Suzuki, N. Kosuge, H. Nagashima, K. Watanabe, H. Inoue, T. Shirai, A Sodium Ion Selective Electrode Based on a Highly Lipophilic Monensin Derivative and Its Application to the Measurement of Sodium Ion Concentrations in Serum, Analytical Sciences, 6 (1990) 227-232. 10.2116/analsci.6.227

[11] K. Suzuki, K. Tohda, Potentiometric ion sensors based on natural carboxylic polyether ionophores and their derivatives, TrAC Trends in Analytical Chemistry, 12 (1993) 287-296. https://doi.org/10.1016/0165-9936(93)87004-H

[12] D. Parmentier, M. Lavenas, E. Güler, S.J. Metz, M.C. Kroon, Selective removal of sodium from alkali-metal solutions with tetraoctylammonium monensin, Desalination, 399 (2016) 124-127. https://doi.org/10.1016/j.desal.2016.08.018

[13] P. Sun, S.G. Pavlostathis, C.-H. Huang, Estimation of environmentally relevant chemical properties of veterinary ionophore antibiotics, Environmental Science and Pollution Research, 23 (2016) 18353-18361. 10.1007/s11356-016-7029-y

[14] J.R. Avilés-Moreno, F. Gámez, G. Berden, J. Oomens, B. Martínez-Haya, Isolated alkali cation complexes of the antibiotic ionophore nonactin: correlation with crystalline structures, Physical Chemistry Chemical Physics, 19 (2017) 14984-14991. 10.1039/C7CP02438J

[15] M.S. Ghauri, J.D.R. Thomas, Evaluation of an ammonium ionophore for use in poly(vinyl chloride) membrane ion-selective electrodes: solvent mediator effects, Analyst, 119 (1994) 2323-2326. 10.1039/AN9941902323

[16] B. Martínez-Haya, J.R. Avilés-Moreno, S. Hamad, J. Elguero, On the ionophoric selectivity of nonactin and related macrotetrolide derivatives, Physical Chemistry Chemical Physics, 19 (2017) 1288-1297. 10.1039/C6CP05324F

[17] B. Martínez-Haya, J.R. Avilés-Moreno, F. Gámez, G. Berden, J. Oomens, Preferential host-guest coordination of nonactin with ammonium and hydroxylammonium, J Chem Phys, 149 (2018) 225101. 10.1063/1.5049956

[18] J.L. Alonso, M.E. Sanz, J.C. López, V. Cortijo, Conformational Behavior of Norephedrine, Ephedrine, and Pseudoephedrine, Journal of the American Chemical Society, 131 (2009) 4320-4326. 10.1021/ja807674q

[19] A.J.M. Valente, A.C.F. Ribeiro, J.M.C. Marques, P.E. Abreu, V.M.M. Lobo, R. Kataky, Transport Properties of Aqueous Solutions of (1R,2S)-(−)- and (1S,2R)-(+)-Ephedrine Hydrochloride at Different Temperatures, Journal of Chemical & Engineering Data, 55 (2010) 1145-1152. 10.1021/je9005757

[20] Q. Zheng, X. Mu, S. Pan, R. Luan, P. Zhao, Ephedrae herba: A comprehensive review of its traditional uses, phytochemistry, pharmacology, and toxicology, J Ethnopharmacol, 307 (2023) 116153. 10.1016/j.jep.2023.116153

[21] R.P. Limberger, A.L.B. Jacques, G.C. Schmitt, M.D. Arbo, Pharmacological Effects of Ephedrine, in: K.G. Ramawat, J.-M. Mérillon (Eds.) Natural Products: Phytochemistry, Botany and Metabolism of Alkaloids, Phenolics and Terpenes, Springer Berlin Heidelberg, Berlin, Heidelberg, 2013, pp. 1217-1237.

[22] Z. Şentürk, N. Erk, S.A. Özkan, C. Akay, Ş. Cevheroğlu, Determination of theophylline and ephedrine HCL in tablets by ratio-spectra derivative spectrophotometry and LC, Journal of Pharmaceutical and Biomedical Analysis, 29 (2002) 291-298. https://doi.org/10.1016/S0731-7085(02)00065-1

[23] N.T. Abdel-Ghani, M.S. Rizk, M. Mostafa, Extractive determination of ephedrine hydrochloride and bromhexine hydrochloride in pure solutions, pharmaceutical dosage form and urine samples, Spectrochim Acta A Mol Biomol Spectrosc, 111 (2013) 131-141. 10.1016/j.saa.2013.03.038

[24] K. Dindar Ç, C. Erkmen, B. Uslu, N.G. Göğer, The Development of Spectrophotometric and Validated Stability- Indicating RP-HPLC Methods for Simultaneous Determination of Ephedrine HCL, Naphazoline HCL, Antazoline HCL, and Chlorobutanol in Pharmaceutical Pomade Form, Comb Chem High Throughput Screen, 23 (2020) 1090-1099. 10.2174/1386207323666200720101835

[25] A.H. Alminshid, H.A. Alalwan, H.A. Abdulghani, M.M. Mohammed, Spectrophotometric study of ephedrine hydrochloride in drug using molecular absorption UV–Visible, Spectrochimica Acta Part A: Molecular and Biomolecular Spectroscopy, 270 (2022) 120828. https://doi.org/10.1016/j.saa.2021.120828

[26] H. Elmansi, F. Belal, G. Magdy, Determination of pholcodine alone or in combination with ephedrine in human plasma using fluorescence spectroscopy, Sci Rep, 12 (2022) 9372. 10.1038/s41598-022-13194-1

[27] A. Roshdy, R. Abdel Salam, G. Hadad, F. Belal, H. Elmansi, Design-assisted HPLC-UV method for therapeutic drug monitoring of pholcodine, ephedrine, and guaifenesin in biological fluids, Sci Rep, 14 (2024) 27933. 10.1038/s41598-024-78793-6

[28] Z. Rabia, I.U. Khan, S. Sharif, S. Farid, H. Iqbal, S.I. Khan, High Performance Liquid Chromatographic–Diode Array Detector Method for Simultaneous Determination of Aspirin, Caffeine and Ephedrine in Weight Loss Formulations, Human Plasma and in vitro Drug–Drug Interaction Studies, Journal of Analytical Chemistry, 75 (2020) 1589-1598. 10.1134/s106193482012014x

[29] M.A. Magdy, R.M. Abdelfatah, Green validated HPTLC and HPLC methods for determination of ephedrine hydrochloride and naphazoline nitrate in the presence of methylparaben, in their pure forms and pharmaceutical formulation, JPC – Journal of Planar Chromatography – Modern TLC, 33 (2020) 141-148. 10.1007/s00764-020-00024-1

[30] F. Pellati, S. Benvenuti, Determination of ephedrine alkaloids in Ephedra natural products using HPLC on a pentafluorophenylpropyl stationary phase, J Pharm Biomed Anal, 48 (2008) 254-263. 10.1016/j.jpba.2007.10.034

[31] J. Zhang, Y. Zhang, Y. Wang, Validated quantification method for five ephedrines in dietary supplements using LC–MS/MS: Application to 503 cases, Journal of Chromatography B, 1039 (2016) 1-7. https://doi.org/10.1016/j.jchromb.2016.11.008

[32] M.H. Spyridaki, P. Kiousi, A. Vonaparti, P. Valavani, V. Zonaras, M. Zahariou, E. Sianos, G. Tsoupras, C. Georgakopoulos, Doping control analysis in human urine by liquid chromatography-electrospray ionization ion

trap mass spectrometry for the Olympic Games Athens 2004: determination of corticosteroids and quantification of ephedrines, salbutamol and morphine, Anal Chim Acta, 573-574 (2006) 242-249. 10.1016/j.aca.2006.04.042

[33] T. Saito, H. Mase, S. Takeichi, S. Inokuchi, Rapid simultaneous determination of ephedrines, amphetamines, cocaine, cocaine metabolites, and opiates in human urine by GC-MS, J Pharm Biomed Anal, 43 (2007) 358-363. 10.1016/j.jpba.2006.06.031

[34] E. Marchei, M. Pellegrini, R. Pacifici, P. Zuccaro, S. Pichini, A rapid and simple procedure for the determination of ephedrine alkaloids in dietary supplements by gas chromatography-mass spectrometry, J Pharm Biomed Anal, 41 (2006) 1633-1641. 10.1016/j.jpba.2006.02.043

[35] S.M. Wang, R.J. Lewis, D. Canfield, T.L. Li, C.Y. Chen, R.H. Liu, Enantiomeric determination of ephedrines and norephedrines by chiral derivatization gas chromatography-mass spectrometry approaches, J Chromatogr B Analyt Technol Biomed Life Sci, 825 (2005) 88-95. 10.1016/j.jchromb.2005.01.016

[36] K.W. Phinney, T. Ihara, L.C. Sander, Determination of ephedrine alkaloid stereoisomers in dietary supplements by capillary electrophoresis, J Chromatogr A, 1077 (2005) 90-97. 10.1016/j.chroma.2005.04.068

[37] L. Mateus-Avois, P. Mangin, M. Saugy, Development and validation of a capillary zone electrophoresis method for the determination of ephedrine and related compounds in urine without extraction, Journal of Chromatography B, 791 (2003) 203-216. https://doi.org/10.1016/S1570-0232(03)00222-8

[38] M.-H.E. Spyridaki, C.J. Tsitsimpikou, P.A. Siskos, C.G. Georgakopoulos, Determination of ephedrines in urine by gas chromatography–mass spectrometry, Journal of Chromatography B: Biomedical Sciences and Applications, 758 (2001) 311-314. https://doi.org/10.1016/S0378-4347(01)00174-8

[39] M.N.M.P. Alçada, J.L.F.C. Lima, M.C.o.B.S.M. Montenegro, PVC membrane electrode without inner reference solution for the direct determination of ephedrine in pharmaceutical preparations, Journal of Pharmaceutical and Biomedical Analysis, 10 (1992) 757-761. https://doi.org/10.1016/0731-7085(91)80076-L

[40] M. Chicharro, A. Zapardiel, E. Bermejo, J.A. Pérez, L. Hernández, Determination of ephedrine in human urine using a glassy carbon electrode, Analytica Chimica Acta, 273 (1993) 361-368. https://doi.org/10.1016/0003-2670(93)80178-N

[41] S.S. Hassan, A.H. Kamel, H. Abd El-Naby, New potentiometric sensors based on selective recognition sites for determination of ephedrine in some pharmaceuticals and biological fluids, Talanta, 103 (2013) 330-336. 10.1016/j.talanta.2012.10.067

[42] E.A. Khudaish, M.T.Z. Myint, J.A. Rather, A solid-state sensor based on poly(2,4,6-triaminopyrimidine) grafted with electrochemically reduced graphene oxide: Fabrication, characterization, kinetics and potential analysis on ephedrine, Microchemical Journal, 147 (2019) 444-453. 10.1016/j.microc.2019.03.041

[43] J.M. Freitas, P.R.L. Silva, R.A.A. Munoz, E.M. Richter, Fast and portable voltammetric method for the determination of the amphetamine adulterant ephedrine in natural over-the-counter weight-loss products, Microchemical Journal, 160 (2021). 10.1016/j.microc.2020.105757

[44] L. Jia, Y. Mao, S. Zhang, H. Li, M. Qian, D. Liu, B. Qi, Electrochemical switch sensor toward ephedrine hydrochloride determination based on molecularly imprinted polymer/nafion-MWCNTs modified electrode, Microchemical Journal, 164 (2021) 105981. https://doi.org/10.1016/j.microc.2021.105981

[45] M.E. Wahba, D. El Wasseef, A.S. Saad, M.E. Draz, Calixarene based portable sensor for the direct assay of indiscriminate ephedrine content of weight loss herbal preparations, RSC Adv, 11 (2021) 12833-12844. 10.1039/d0ra10254g

[46] M.-R. Huang, G.-L. Gu, Y.-B. Ding, X.-T. Fu, R.-G. Li, Advanced Solid-Contact Ion Selective Electrode Based on Electrically Conducting Polymers, Chinese J. Anal. Chem., 40 (2012) 1454-1460. 10.1016/s1872-2040(11)60572-0

[47] M. Fibbioli, W.E. Morf, M. Badertscher, N.F.d. Rooij, E. Pretsch, Potential Drifts of Solid-Contacted Ion-Selective Electrodes Due to Zero-Current Ion Fluxes Through the Sensor Membrane, Electroanalysis, 12 (2000) 1286-1292. https://doi.org/10.1002/1521-4109(200011)12:16<1286::AID-ELAN1286>3.0.CO;2-Q

[48] Y. Shao, Y. Ying, J. Ping, Recent advances in solid-contact ion-selective electrodes: functional materials, transduction mechanisms, and development trends, Chem Soc Rev, 49 (2020) 4405-4465. 10.1039/c9cs00587k

[49] Y. Lyu, S. Gan, Y. Bao, L. Zhong, J. Xu, W. Wang, Z. Liu, Y. Ma, G. Yang, L. Niu, Solid-Contact Ion-Selective Electrodes_ Response Mechanisms, Transducer Materials and Wearable Sensors, membranes, 10 (2020) 128-152. 10.3390/membranes10060128

[50] I. Švancara, K. Vytřas, K. Kalcher, A. Walcarius, J. Wang, Carbon Paste Electrodes in Facts, Numbers, and Notes: A Review on the Occasion of the 50-Years Jubilee of Carbon Paste in Electrochemistry and Electroanalysis, Electroanalysis, 21 (2009) 7-28. 10.1002/elan.200804340

[51] C. Hu, H. Shengshui, Carbon Nanotube-Based Electrochemical Sensors: Principles and Applications in Biomedical Systems, Journal of Sensors, 2009 (2009) 187615. https://doi.org/10.1155/2009/187615

[52] A.J.S. Ahammad, J.-J. Lee, M.A. Rahman, Electrochemical Sensors Based on Carbon Nanotubes, Sensors, 9 (2009) 2289-2319. https://doi.org/10.3390/s90402289

[53] C. Wardak, K. Pietrzak, K. Morawska, Nanocomposite of copper oxide nanoparticles and multi-walled carbon nanotubes as a solid contact of a copper-sensitive ion-selective electrode: intermediate layer or membrane component–comparative studies, Applied Nanoscience, 13 (2023) 7017-7028. 10.1007/s13204-023-02846-x

[54] N.A. Abdallah, H.F. Ibrahim, Electrochemical determination of Saxagliptin hydrochloride with MWCNTs/CuO/4′aminobenzo-18-crown-6-ether composite modified carbon paste electrode, Microchemical Journal, 147 (2019) 487-496. https://doi.org/10.1016/j.microc.2019.03.060

[55] I. Sharafeldin, S. Garcia-Rios, N. Ahmed, M. Alvarado, X. Vilanova, N.K. Allam, Metal-decorated carbon nanotubes-based sensor array for simultaneous detection of toxic gases, Journal of Environmental Chemical Engineering, 9 (2021) 104534. https://doi.org/10.1016/j.jece.2020.104534

[56] E.H. Espinosa, R. Ionescu, B. Chambon, G. Bedis, E. Sotter, C. Bittencourt, A. Felten, J.J. Pireaux, X. Correig, E. Llobet, Hybrid metal oxide and multiwall carbon nanotube films for low temperature gas sensing, Sensors and Actuators B: Chemical, 127 (2007) 137-142. https://doi.org/10.1016/j.snb.2007.07.108

[57] N.A. Abdallah, Novel Calcium Potentiometric Selective Electrode Based on Lisinopril Functionalized Multi-walled Carbon Nanotubes-NiO Nanocomposite, International Journal of Electrochemical Science, 16 (2021) 210815. https://doi.org/10.20964/2021.08.21

[58] L. Ernö, U. Yoshio, Performance evaluation criteria for preparation and measurement of macro- and microfabricated ion-selective electrodes (IUPAC Technical Report), Pure Appl. Chem., 80 (2008) 85-104. 10.1351/pac200880010085

[59] R.A. Al-Haidari, N.A. Abdallah, M.M. Al-Oqail, E.S. Al-Sheddi, S.M. Al-Massarani, N.N. Farshori, Nanoparticles based solid contact potentiometric sensor for the determination of theophylline in different types of tea extract, Inorganic Chemistry Communications, 119 (2020) 108080. https://doi.org/10.1016/j.inoche.2020.108080

[60] Q. Chemical Computing Group Inc.: Montreal, Canada, Molecular Operating Environment, Montreal, QC, Canada, 2024.

[61] A. Economou, H. Botitsi, S. Antoniou, D. Tsipi, Determination of multi-class pesticides in wines by solid-phase extraction and liquid chromatography-tandem mass spectrometry, J. Chromatogr. A, 1216 (2009) 5856-5867. 10.1016/j.chroma.2009.06.031

[62] H. Wang, Z.-H. Zhang, H.-M. Zhang, Z.-Y. Hu, S.-L. Li, X.-W. Cheng, Novel synthesizing and characterization of copper matrix composites reinforced with carbon nanotubes, Materials Science and Engineering: A, 696 (2017) 80-89. https://doi.org/10.1016/j.msea.2017.04.055

[63] D.-W. Kim, K.-Y. Rhee, S.-J. Park, Synthesis of activated carbon nanotube/copper oxide composites and their electrochemical performance, Journal of Alloys and Compounds, 530 (2012) 6-10. https://doi.org/10.1016/j.jallcom.2012.02.157

[64] J.E. Jeronsia, D.J.V. Raj, L.A. Joseph, K. Rubini, S.J. Das, In Vitro Antibacterial and Anticancer Activity of Copper Oxide Nanostructures in Human Breast Cancer Michigan Cancer Foundation-7 Cells, Journal of Medical Sciences, 36 (2016) 145-151. 10.4103/1011-4564.188899